Surface & Coatings Technology 422 (2021) 127555

Contents lists available at ScienceDirect

Surface & Coatings Technology

journal homepage: www.elsevier.com/locate/surfcoat

Tribo-mechanical and cellular behavior of superficially modified porous titanium samples using femtosecond laser

Paloma Trueba [a], Mercè Giner [b,*], Ángel Rodríguez [c], Ana M. Beltrán [a], José M. Amado [c], María J. Montoya-García [d], Luisa M. Rodríguez-Albelo [a], Yadir Torres [a]

[a] Departamento de Ingeniería y Ciencia de los Materiales y del Transporte, Universidad de Sevilla, Escuela Politécnica Superior, Calle Virgen de África, 7, 41011 Sevilla, Spain
[b] Departamento de Citología e Histología Normal y Patológica, Universidad de Sevilla, Avda Dr. Fedriani s/n, 41009 Sevilla, Spain
[c] Escuela Politécnica Superior, Universidade da Coruña, Mendizábal s/n, E-15403 Ferrol, Spain
[d] Departamento de Medicina, Universidad de Sevilla, Avda. Dr. Fedriani s/n, Sevilla 41009, Spain

ARTICLE INFO

Keywords:
Porous titanium
Femtosecond laser
Surface modification
Instrumented micro-indentation
Scratch resistance
Cellular behavior

ABSTRACT

In this work, the surface of porous titanium samples obtained by the space-holder technique was treated with a femtosecond laser to improve their osseointegration. Instrumented micro-indentation and scratch test were implemented to evaluate the tribo-mechanical behavior of the surface of the modified samples. A detailed study of micro-hardness, stiffness, scratch resistance and elastic recovery was performed. Also, in vitro analysis was carried out to evaluate the cellular behavior. Modified samples showed less ALP activity, which could indicate a greater differentiation of the cells. The cell culture was similar in all cases although more differentiated morphology, good cell adherence and biological response were observed on treated samples. Finally, the discs with a pore size between 100–200 μm present being potential candidates for the replacement of small portions of damaged cortical bone tissues.

1. Introduction

Titanium (Ti) and its related alloys are widely used as a material for dental and orthopedic implants due to their mechanical properties, excellent corrosion resistance in physiological fluids and good biocompatibility [1–4]. Despite these advantages, Ti presents some drawbacks for its application as biomaterial. On the one hand, in terms of biomechanical properties, the difference in Young's modulus between the material and the cortical bone can originate stress shielding problems that may cause inadequate bone remodeling and eventual implant failure interface that limits its osseointegration capacity and can cause loosening of the implant [5,6]. On the other hand, Ti is generally considered as bio-inert, which can lead to the formation of a fibrous tissue film around the implant, which may cause it to loosen.

Porous titanium implants constitutes an interesting approach to reduce the difference in stiffness between the implant and the bone, being able to avoid stress shielding problems [7–10]. Furthermore, it has been shown that interconnected porous structures with diameter pores greater than 100 μm allow tissue growth inside the pores, creating a strong mechanical interlock [11–13]. However, the reduction of the strength and fatigue resistance of porous materials could also be a drawback. Therefore, it is necessary to correctly design the porous structure (pore size, porosity, pore distribution) to achieve a good balance between strength and stiffness and ensure that the performance of the implant will be optimal under real service conditions [14,15].

One of the most common approaches to improve bioactivity is the modification of the topography of the surface, for example, by microtextured [16–20]. Currently, it has been proposed that structures at the nanometric level can provide additional value with respect to purely micrometric structures, since they better replicate the texture of the bone surface and increase interaction with proteins, promoting cell adhesion [21–23]. Several studies have shown that nanostructures can improve the differentiation and adhesion of mesenchymal stem cells [24–26]. Furthermore, since nanofeatures differently interact with various cell types, they have been proposed to prevent the proliferation and adhesion of bacteria [27,28]. However, this field of research is still in its early stages and further studies are required to fully comprehend how different cell types and bacteria react to nanoscale features and

* Corresponding author.
E-mail addresses: ptrueba@us.es (P. Trueba), mginer@us.es (M. Giner), angel.rcarballo@udc.es (Á. Rodríguez), abeltran3@us.es (A.M. Beltrán), jose.amado.paz@udc.es (J.M. Amado), pmontoya@us.es (M.J. Montoya-García), lralbelo@us.es (L.M. Rodríguez-Albelo), ytorres@us.es (Y. Torres).

https://doi.org/10.1016/j.surfcoat.2021.127555
Received 14 June 2021; Received in revised form 20 July 2021; Accepted 21 July 2021
Available online 25 July 2021

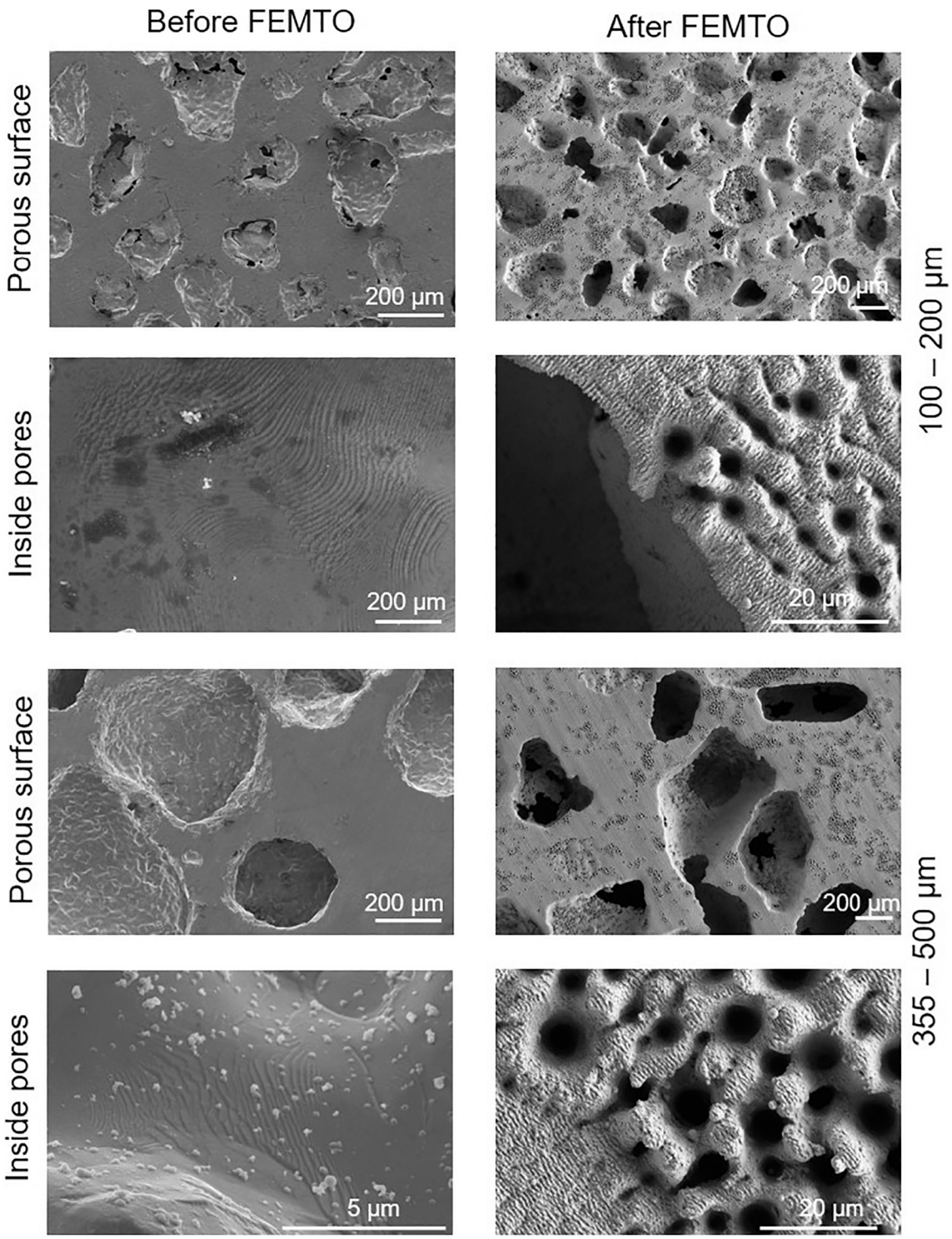

Fig. 1. SEM micrographs before and after and the modification by femtosecond laser of the surface and inside the pores for the two studied pores range size (100–200 and 355–500 µm).

clearly show their advantages over their micrometer-scale analogues in long-term implant behavior [29–32].

In this previous scenario, laser texturing allows the generation of micro- and nano-scale textures on material surfaces [33,34]. This technology has several advantages, since it can produce different geometric typologies on the surface with great precision and without generating waste, while being fast and consuming small amount of material [35]. Traditionally, in the field of laser micromachining, the lasers were long pulsed, typically in the nanosecond and picosecond range. Recently, the increasing availability of ultrashort femtosecond lasers has highlighted the advantages that this technology has over traditionally used long pulse lasers. With this processing technology, the interaction times between laser and material are much shorter, so the material is less affected and damaged, allowing obtaining machining with high quality and much greater precision [36–39]. Another great advantage that femtosecond lasers present for surface modification is that they allow the generation of a much larger variety of micro and nano-structures compared to those that can be obtained with long pulses [40].

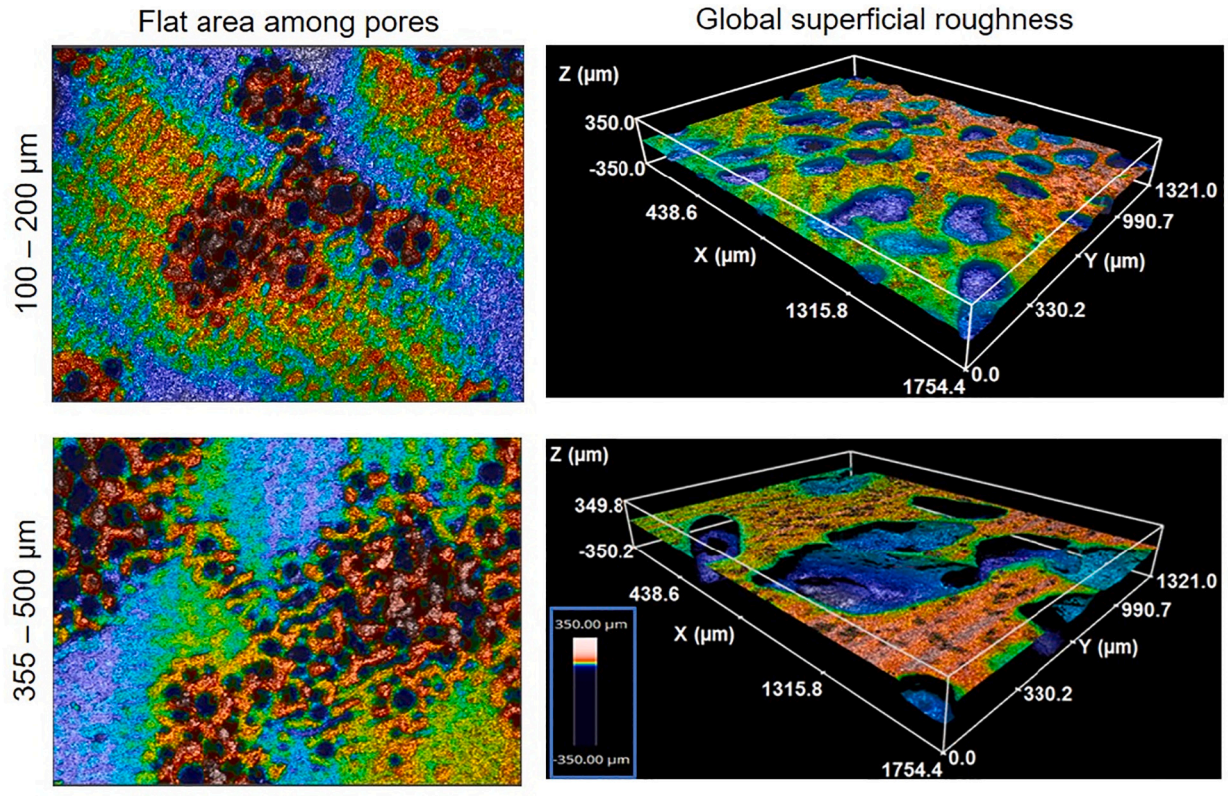

	Flat area among pores		Global superficial roughness	
	Fully-dense	100 – 200 µm	355 – 500 µm	100 – 200 µm	355 – 500 µm
S_a (µm)	1.0	0.47	1.02	2.61	6.03
S_q (µm)	1.52	0.82	1.54	7.21	13.52

Fig. 2. 2D and 3D CLM images of the surface of both studied pore range size. Inset: S_a and S_q parameters of the fully-dense and the two porous substrates for the flat area and in global surface modified by femtosecond laser. Common scale bar.

In a previous work, authors showed the feasibility to generate hierarchical micro-nano-structures on the surface of fully-dense and porous titanium substrates using femtosecond laser texturing [41]. The authors characterized the morphology, roughness and porosity of the samples and the surface structures were compared before and after laser treatment. However, in this work the authors perform a detail analysis of the tribo-mechanical behavior of superficially modified porous titanium substrates, as well as an in vitro study to evaluate the capacity to improve cell behavior of the proposed methods. Biological cultures were performed on the surface of the samples to evaluate cell viability, proliferation, differentiation and morphology. The results allowed evaluating and comparing the performance of the different modified surfaces obtained in terms of the biofunctional enhancement of the implants.

2. Materials and methods

2.1. Fabrication of the porous titanium substrates

Fully-dense and porous commercially pure titanium (c.p. Ti -Grade IV, provided by SEJONG Materials Co. Ltd.) discs were manufactured using the powder metallurgy technology. The fully-dense sample was obtained by pressing and sintering the powder at 1300 MPa and 1300 °C, respectively. The porous samples were produced by the space-holder technique using two different particle size ranges: 100–200 µm and 355–500 µm to evaluate the effect of pore size on micro-mechanical and biological behavior. In both cases the Ti powder was mixed with 40 vol% of spacer particles (NH_4HCO_3). Afterwards, the mixture was pressed at 800 MPa and then, the spacer was removed using a low vacuum furnace (Heraeus, Hanau, Germany) (10^{-2} mbar) in two stages (60 °C and 110 °C) during 12 h each. Finally, the porous green samples were sintered at 1250 °C in a molybdenum chamber furnace (Termolab–Fornos Eléctricos, Lda., Águeda, Portugal) under high vacuum atmosphere ($\sim 10^{-5}$ mbar) for 2 h. Before performing the surface modification, the surface of the samples was grinded and polished with magnesium oxide (MgO) and hydrogen peroxide (H_2O_2). The porosity fraction, size and morphology of the pores were preserved after preparation.

2.2. Surface modification by femtosecond laser texturing

Laser surface modification was performed by means of a femtosecond Yb-doped fiber laser (Spirit 1040–4, Spectra-Physicas, Santa Clara, CA, USA), with a wavelength of 1040 nm and 396 fs pulses at a repetition rate of $f = 100$ kHz, with maximum pulse energy of 49.7 µJ. A

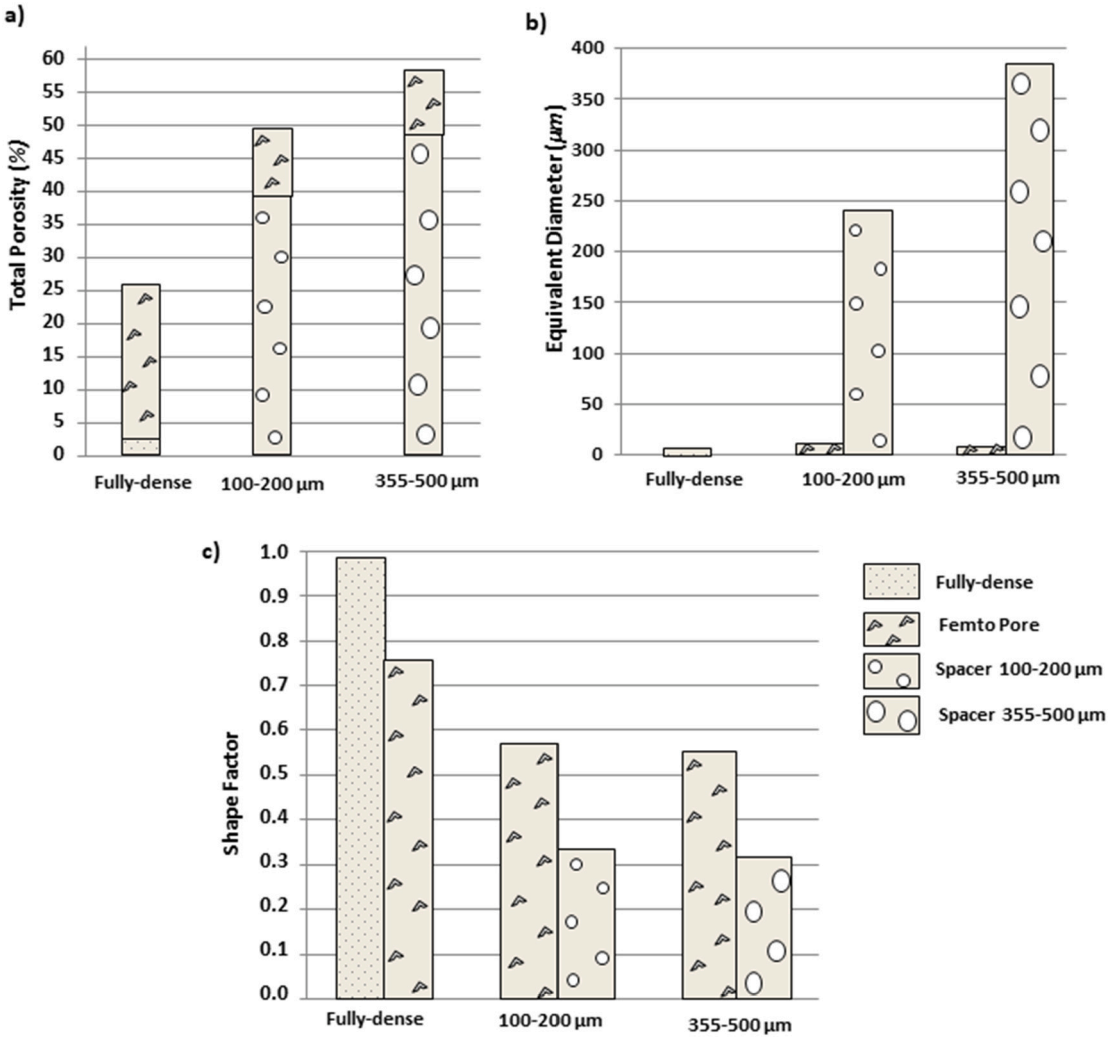

Fig. 3. Porosity parameters measured obtained by image analysis, for the two pore populations: macro-pores obtained by spacer holder technique and micro-pores obtained by femtosecond laser treatment: a) total porosity, b) equivalent diameter and c) shape factor.

scanning system consisting of galvanometer scanners and an F-Theta lens (f = 160 mm) was used to obtain a constant beam radius of $w_o = 12$ µm on the working surface. The system allows the movement of the laser beam on the surface according to programmed plane trajectories. Laser processing was performed in air and an Ar jet was directed to the area being processed to prevent any undesirable oxidation of the surface.

The porous titanium surface was irradiated by the laser using parallel rectilinear paths. Process parameter selection was based on a set of preliminary scans in which different combinations of laser power, scan speed and number of irradiations over the area were tested. The parameters selected were the ones that allowed obtaining two laser generated structures simultaneously on the surface: columnar micro structures or micro pillar and laser-induce periodic surface structures (LIPSS). The pulse energy under this criterion was $E_p = 49.7$ µJ and the scanning speed $v = 960$ mm/s, corresponding to a fluence of $F = 21.98$ J/cm^2. The hatch distance between lines was $d = 12$ µm and the number of times that each area was scanned was $N_r = 20$. Using these parameters, the number of pulses per spot on the surface was $PPS = 100$.

2.3. Microstructural and micromechanical characterization

Total porosity (P_T), equivalent diameter (D_{eq}) and shape factor (F_f) of the pores were measured by quantitative image analysis (IA) using a Nikon Epiphot optical microscope (Nikon, Tokyo, Japan) coupled with a Jenoptik Progres C3 camera (Jenoptik, Jena, Germany) and Image-Pro Plus 6.2 analysis software [8,42,43]. The image analysis allowed differentiating and evaluating the porosity caused by the spacer particles and that generated by the laser surface treatment, separately.

The surface topography of the samples was characterized by scanning electron microscopy (FEI Teneo, FEI, Eindhoven, The Netherlands). The morphology of the pores from the spacer particles and that of the microstructures and nanostructures present on the surface was examined before and after the laser treatment as well as the roughness of the surfaces was measured using confocal laser scanning microscopy (CLM) (Sensofar Sneox, Sensofar, Glonn, Germany) allowing two-dimensional (2D) and three-dimensional (3D) images. Roughness was evaluated in the total surface and in the characteristic areas of the samples: flat area between the pores and inside the pores. To quantify the surface roughness, the arithmetical mean deviation (S_a) and the root mean square height (S_q) were used.

Also, the micro-tribomechanical behavior of the samples was evaluated by instrumented micro-indentation (*P-h* curves) and scratch tests. Loading-unloading tests were performed using a Microtest machine (MTR3/50-50/NI) equipped with a Vickers indenter, at an applied load rate of 1 N/min, a maximal load of 1 N and a holding time of 10 s. The micro-hardness and Young's modulus were calculated from the loading-unloading curves obtained using the Oliver and Pharr method [44]. Indentations were performed in different areas of the samples to study

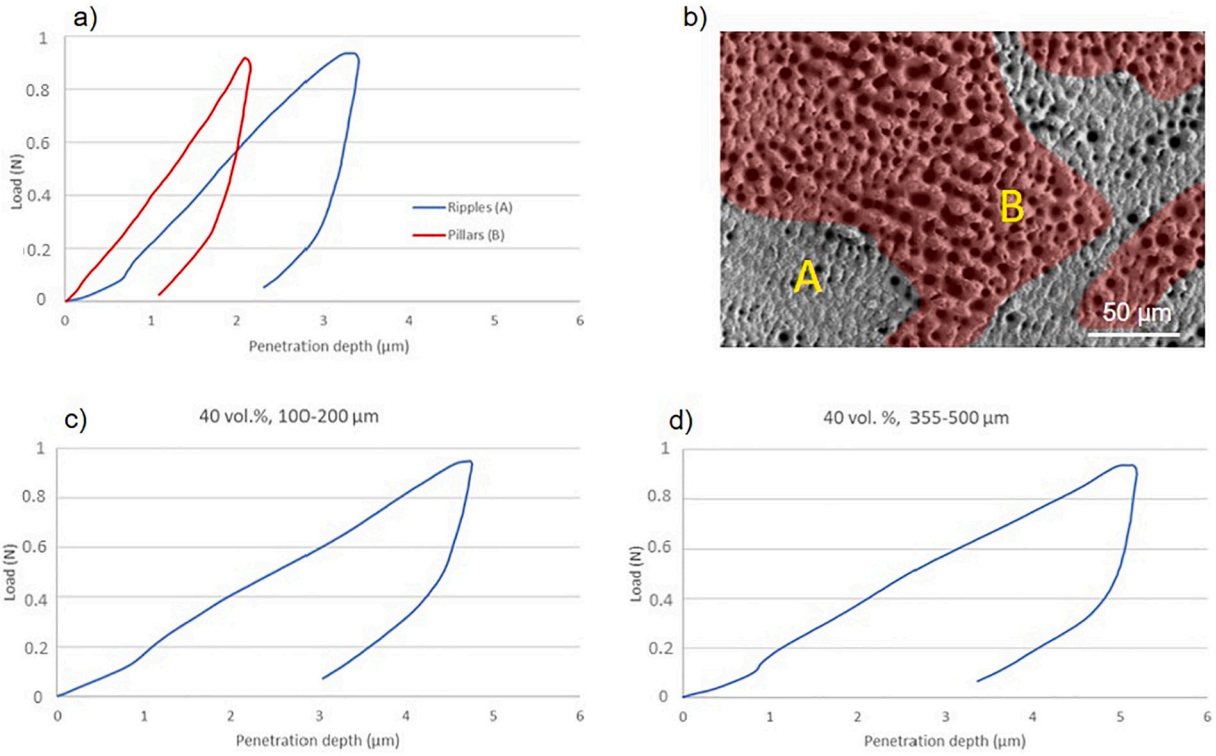

Fig. 4. Loading-unloading curves (*P-h* curves) of superficially modified by femtoseconds a) fully-dense, c and d) porous c.p. Ti substrates. SEM image (b) illustrates the nano-ripples and pillars on the fully-dense sample.

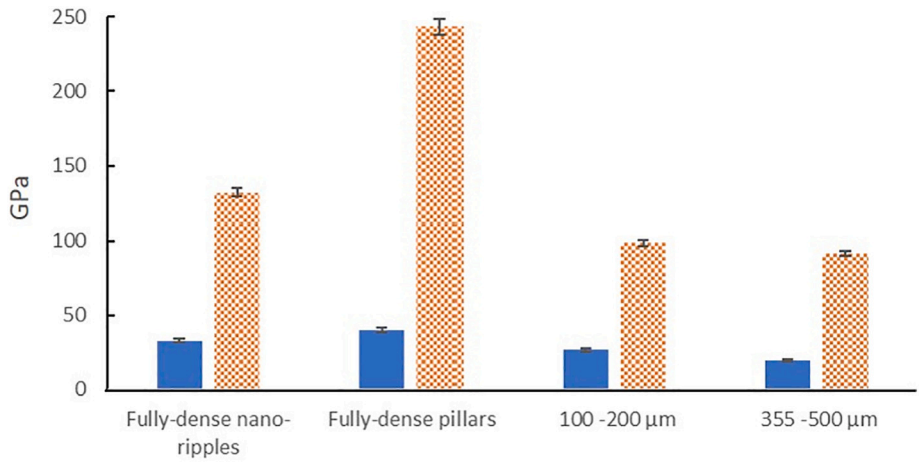

Fig. 5. Modulus of young and micro-hardness of the surface of the discs (fully-dense and porous) modified with the femtosecond laser treatment.

Table 1
Characteristic parameters of *P-h* curves for the femtoseconds modified c.p. Ti substrates.

		Fully-dense		100–200 μm	355–500 μm
		Ripples	Pillars		
Penetration depth (μm)	Maximum	3.4 ± 0.1	2.2 ± 0.1	4.8 ± 0.2	5.2 ± 0.2
	Permanent	2.2 ± 0.1	1.0 ± 0.1	2.8 ± 0.1	3.1 ± 0.1
Elastic recovery	Absolute (μm)	1.3 ± 0.1	1.2 ± 0.1	2.0 ± 0.1	2.1 ± 0.1
	Relative (%)	37 ± 1.2	53 ± 1.8	41 ± 1.4	40 ± 1.4

the influence of macro-porosity and surface treatment on micro-mechanical behavior.

Scratch test were performed on the surface of the substrates using a MICROTEST commercial device (MTR3/50-50/NI) with a Rockwell diamond tip of 200 μm diameter applying a maximum constant load of 3 N at a rate of 0.5 mm min^{-1} for 3 mm of groove scar, following the ASTM C1624–05 standard [45]. The normal load was continuously recorded during in situ scratching. Results were given as scratch penetration—-load curves. Besides, the real penetration depth of the groove scar (permanent deformation) and an estimation of the elastic recovery were evaluated. Before the scratch test, the samples were scanned to evaluate the roughness profile of the surface, determining the values of: the arithmetic average of the absolute values of all points of the profile (R_a), the root mean square of the values of all points of the profile (R_q), the maximum peak-to-valley height of the entire measurement trace (R_y),

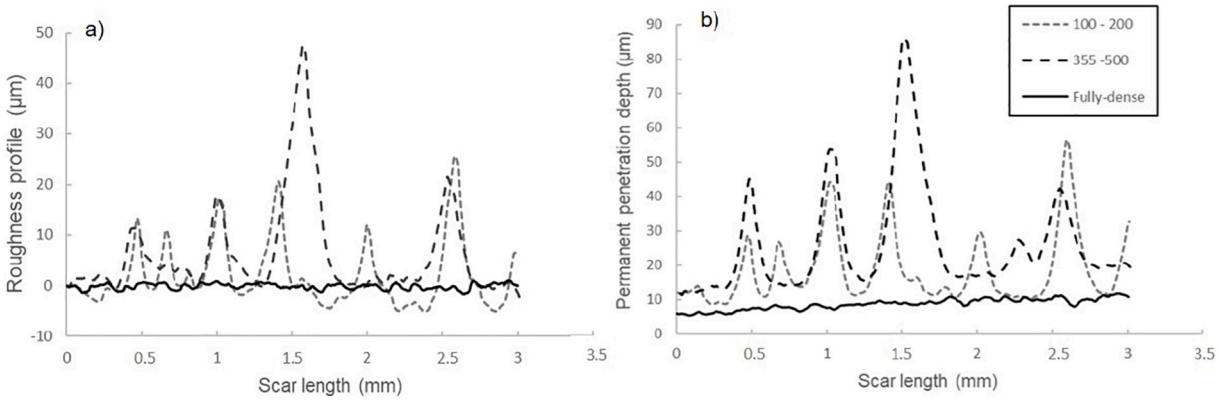

Fig. 6. a) Roughness profile, and **b)** permanent penetration depth.

and the arithmetic average of the maximum peak-to-valley height of the roughness values of five consecutive sampling sections over the filtered profile (R_z). At least three measurements were performed for each type of material and area of interest.

2.4. In-vitro cell behavior

MC3T3E1, a murine pre-osteoblast cell line (CRL-2593 from American Type Culture Collection (ATCC), Manassas, USA), was used to analyze the potential influence of surface modified with femtosecond in the bone cells, in Ti disc with or without porosity, on cell metabolism and viability during the cell adhesion and proliferation process. Results were compared to the same substrates but without surface modification.

2.4.1. Cell culture

Routine passaging of the cell line was performed on 25 cm^2 flasks with Minimum Essential Medium (αMEM), containing 10% fetal bovine serum plus antibiotics (100 U/mL penicillin and 100 mg/mL streptomycin sulphate) (Invitrogen, Carlsbad, USA). Sample discs were autoclaved at 121 °C for 30 min and were then placed onto a 24-well plate. Osteoblast cells were seeded at a cellular density of 30,000 cells/cm^2 per sample and in 800 µL of pre-warmed culture medium. Plates were kept at 37 °C in a humidified 5% CO_2 atmosphere and as a control, triplicate blank TCP (Tissue culture plastic) and fully dense pure titanium discs were employed as negative and positive controls on the same plate for each time of period.

At 48 h of osteoblast cultured, the cell media was changed to osteogenic media (α-MEM medium) supplemented with 10 mM of ascorbic acid (Merck, Darmstadt, Germany) and 50 µg/mL [1–55] of β-glycerophosphate (StemCell Technologies, Vancouver, Canada). The in-vitro cell experiments were carried out at 21 days of cell incubation in which the samples were transferred onto a new 24-well plate to prevent counting non-attached or attached cells on the well plate.

2.4.2. Cell viability and proliferation assay

Cell proliferation and viability tests were evaluated using AlamarBlue® reagent (Invitrogen, Carlsbad, USA). In accordance with the manufacturer's protocol, new fresh media (800 µL) and 80 µL of AlamarBlue® reagent were added and the plate was incubated for 1.5 h at 37 °C in dark conditions. The absorbance at 570 nm (oxidized) and 600 nm (reduced) (TECAN, Infinity 200 Pro) was subsequently recorded.

2.4.3. Cell differentiation by alkaline phosphatase (ALP) evaluation

MC3T3 differentiation levels were evaluated through alkaline phosphatase (ALP) activity, using the Alkaline Phosphatase Assay kit (Colorimetric) (Abcam, Cambridge, United Kingdom). The assay was performed in triplicate according to the manufacturer's protocol. The absorbance at 405 nm of 4-nitrophenol was measured in a 96-well microplate reader. Data was expressed as µmol/min/ml of *p*-Nitrophenyl Phosphate (pNPP).

2.4.4. Cell morphology

Cell behavior at 21 days was evaluated by the acquisition of images with a scanning electron microscopy (SEM) (Zeiss EVO LS 15 scanning electron microscope (Zeiss, Oberkochen, Germany) with an acceleration voltage of 10 kV. The samples were fixed in 10% formalin, which was followed by a dehydration step with ethanolic solutions and then coated by gold-coating using a sputter coater (Pelco 91000, Ted Pella, Redding, CA, USA).

2.5. Statistical analysis

All experiments were performed in triplicate to ensure reproducibility. The results were expressed in terms of mean and standard deviation to perform two-way ANOVA followed by Tukey's post-test using SPSS v.22.0 for Windows (IBM Corp., Armonk, NY, USA). The significance level was considered at p values of $p < 0.05$ (*) and $p < 0.01$ (**).

3. Results and discussion

The porous c.p. Ti substrates were characterized before and after the surface modification to evaluate the porosity parameters (morphology, distribution and average pore size, as well as the roughness of the surface and inner walls of the pores). Fig. 1 displays SEM images before and after femtosecond laser irradiation of the porous samples. All the samples showed certain roughness associated to the fabrication technique. After the femtosecond laser, the modification of the surface at micro and nanoscale was evident with the generation of micro-holes and microcolumns, for the entire surfaces, both in the area among macro-pores and inside them. No differences were observed for the different macro-pore range sizes. Higher magnification images clearly displayed that the entire surface was covered by periodic aligned nanometric ripples (LIPSS), which are produced when the surface is irradiated using ultrashort laser pulses (see Fig. 1, inside pores of larger pore size) [40]. The resulting surface is therefore composed of a hierarchical structure with features belonging to different size ranges. These types of structures are of interest since they can better mimic the structure of the bone at different length scales [46,47].

The roughness of the samples modified with the femtosecond laser treatment was analyzed using confocal laser microscopy (CLM) in 2D and 3D. The surface roughness was measured in terms of S_a and S_q (Fig. 2). The results reveal a clear increment of the roughness due to the surface patterns originated by the femtosecond laser and also with the effect of the macro pores size (compare the values for the fully-dense, 100–200 µm and 255–500 µm). The roughness measured on the fully-dense sample was similar to the roughness measured on the flat area

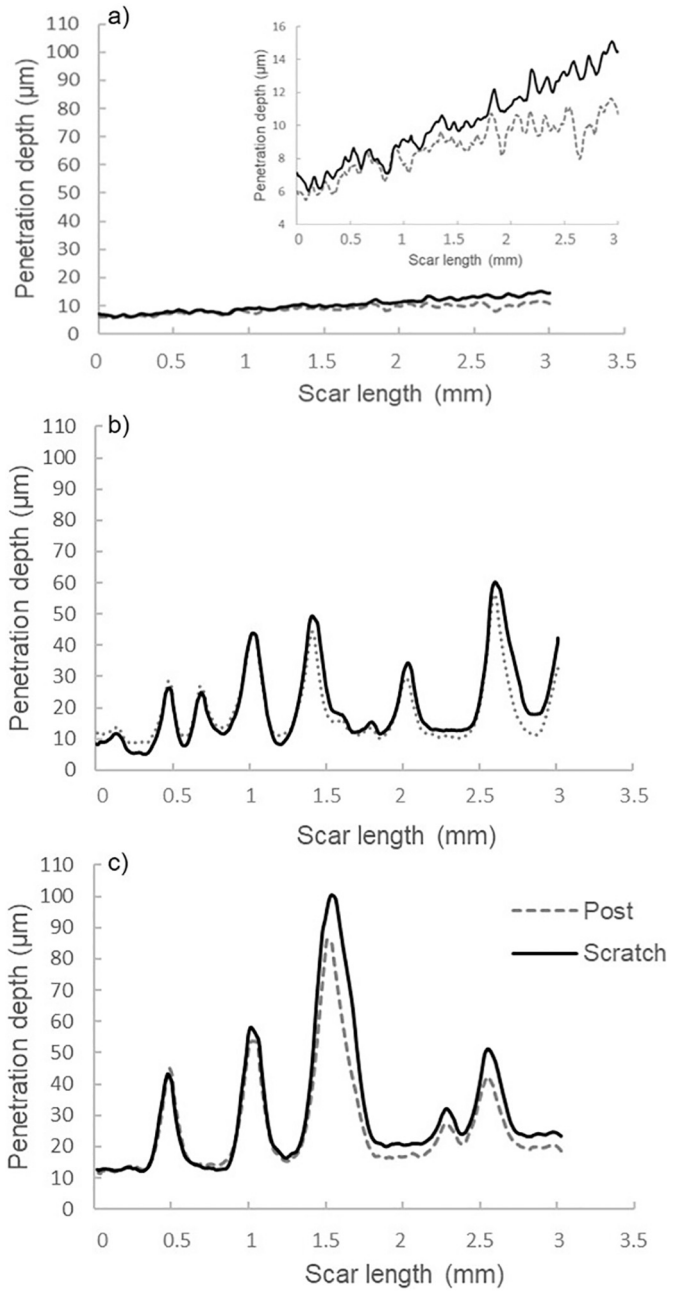

Fig. 7. Penetration depth during and after the scratch tests for the c.p. Ti substrates: a) fully-dense, b) 40 vol% 100–200 μm, and c) 40 vol% 355–500 μm. Inset: magnification of the graphic.

Table 2
Surface roughness parameters of the studied samples. Error below 0.1%.

	Fully-dense	100–200	355–500
R_a (μm)	1.33	7.16	9.22
R_q (μm)	1.47	9.60	13.34
R_z (μm)	2.49	30.72	50.49
R_y (μm)	2.49	30.73	50.52

between macro-pores for the sample with larger pore range size (355–500 μm), indicating that the laser treatment had a similar effect on both types of samples. It might be related to the fact that the area of Ti matrix among larger macro-pores was statistically comparable to the superficial area of the fully-dense discs. Therefore, the roughness

Table 3
Absolute and relative permanent plastic deformation values.

		Fully-dense	100–200 μm	355–500 μm
Permanent deformation depth	Maximum (μm)	11.6	56.3	86.2
	Average (μm)	8.7	18.7	26.2
Elastic recovery	Absolut (μm)	1.5 ± 1.2	1.6 ± 2.5	4.2 ± 4.3
	Relative (%)	17 ± 3	6 ± 3	13 ± 4

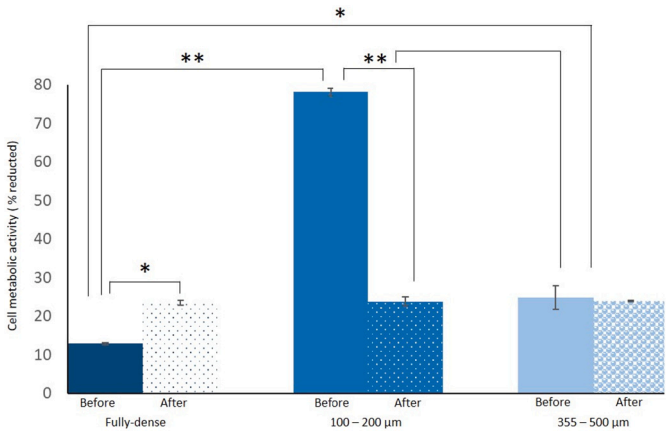

Fig. 8. Cell metabolic activity in adhesion and proliferation stages. Significance level at p value < 0.05 (*) or <0.001 (**).

created by the femtosecond laser treatment was similar in both cases. However, it did not happen for smaller macro-pores range size since the less Ti matrix was affected by the laser.

Fig. 3 shows the trend of the values of P_T, D_{eq} and F_f, obtained by IA, for fully-dense substrates and porous substrates, after surface modification. The study allowed discriminating three pore populations: the micro-pores associated with the sintering process, the macro-pores obtained by spacer particles and the micro-pillars due to the femtosecond laser treatment. It was observed (Fig. 3a) that the percentage of P_T obtained by femtosecond laser treatment was higher in the fully-dense substrates (23.2%), than porosity substrates obtained by spacer particles (10.4% for 100–200 μm and 9.3% for 355–500 μm). This trend could be explained because the flat area in fully-dense was greater than in porous samples. In samples obtained using spacers, the presence of macro-pores was the predominant factor when calculating the total porosity even after the femtosecond treatment. Equivalent diameter measurements were made independently for each type of pore (Fig. 3b). On one hand, the micro-porosity obtained by femtosecond laser treatment had D_{eq} = 3.2 μm and on the other hand the macro-porosity generated by the spacers had D_{eq} = 237 and 372 μm for the 100–200 μm and 355–500 μm samples, respectively. As expected, the measured diameter was larger as the size of the spacer increased. Concerning F_f values (Fig. 3c), it was worth to highlight the larger roundness of the micro-pores inherent to the sintering stage (0.97), which decreases when the micro-pillars generated with the femtosecond treatment were analyzed (0.74 for fully-dense sample and 0.58 and 0.56 for 100–200 μm and 355–500 μm samples, respectively). On the other hand, it was observed that after femtosecond laser treatment, the macro-pores obtained with the spacers were less rounded than before, with values further away from 1 (0.33 and 0.31 for 100–200 μm and 355–500 μm, respectively, compared with the 0.6 values obtained for the original macro-pores) [48]. This fact could be related to the modification that occurs in the contours of the macro-pores by the action of the laser.

The micro-tribomechanical behavior of the c.p. Ti porous substrates superficially modified by femtosecond laser irradiation was measured by

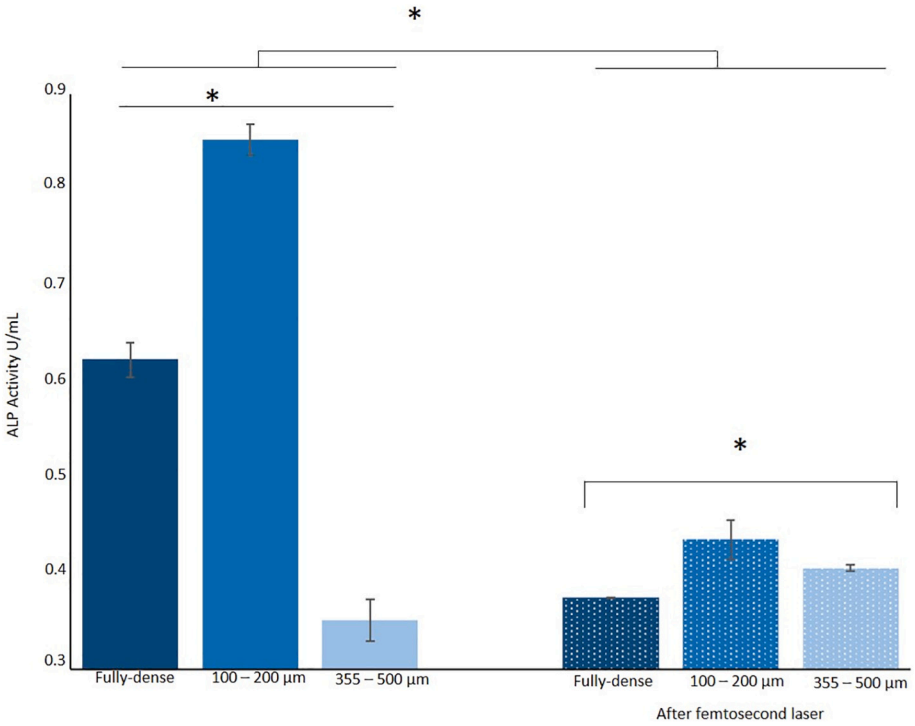

Fig. 9. Cell differentiation of osteoblasts, in-vitro evaluation of alkaline phosphatase enzyme (ALP) activity measured as U/mL. Statistical differences are indicated at $p < 0.05$ *.

P-h curves and scratch tests. Concerning the *P-h* curves, micro-indentations (Fig. 4) were performed on the fully-dense samples, discriminating two areas according to the characteristic structures presented after the femtosecond laser: nano-ripples and micro-structures/micropillars. The analysis of the curves indicated a greater microhardness and stiffness in the area with the pillars, which could be associated with a greater thickness of the modified layer in this area. It is worth to mention, that laser treatment generated a certain fusion of the material and a potential hardening during the cooling of this modified layer and oxidation. The analyses of the *P-h* curves and scratch-test (Fig. 5) allowed checking that penetration depth, HV and E were affected by the effect of the size of the macro-porosity due to the spacer particles (Table 1). A kind of pseudo-creep behavior was also observed in the porous samples with larger pore size (see the plateau area of the curve). In general, the trends of Young's modulus and Vickers micro-hardness values were consistent with the content and size of the macro-pores, as well as with the metallurgical processes and/or morphological features of the patterns and pillars inherent to the process of surface modification with the femtosecond laser treatment.

Fig. 6a displays the linear roughness profile on the surface of the studied samples (fully-dense and porous), while the Fig. 6b corresponds to the scratch resistance measure in terms of permanent penetration depth. Scratch resistance was also measured as permanent penetration depth (Fig. 7). Main parameters are summarized in Table 3, such as the permanent deformation and the elastic recovery, as a value of the resistance to penetration. The trends of the roughness values were consistent with the size of the macro-pores inherent to the spacer particles and with the patterns texture generated with the femtosecond laser treatment. Micro-hardness and the degree of surface porosity determined the scratch resistance and elastic recovery of surface-treated discs (Table 2).

Viability studies were directly related to the biocompatible and cytotoxic properties of the material. Specifically, the percentage of reduced substrate indicated the metabolic activity of the cells [49]. Results showed a remarkable increased in metabolic activity that corresponds to an increase in cell proliferation. As it is displayed in Fig. 8, all cultures presented a metabolic activity greater than 12%, indicating an optimal degree of biocompatibility as well as absence of toxicity. Surface-modified discs presented a similar viability, around 25% without observing significant differences among them. Comparing the metabolic activity of the modified and non-modified discs, it was observed that all of them had twice metabolic activity than the fully-dense discs. This difference was considered statistically significant. These results agree with those published by other authors who have stated greater viability in MG63 or INT407 [50,51] after modification the surface with femtosecond laser, and greater osseointegration in bone prostheses in animals [51]. On the other hand, Civantos et al. also reported that increasing the porosity of the surface with a pore size of 100–200 µm, cell viability improved compared to fully-dense discs [52].

As shown in Fig. 9, ALP activity of the cells in the surface-modified discs were significantly different, indicating variable cellular responses including the differentiation and functions of MC3T3 cells. Knowing that ALP is an early marker of osteoblastic proliferation, and the peak of ALP activity is the beginning of the mineralization process, the low values that were found may be associated to a greater differentiation of the osteoblastic cell. The highest ALP activity occurred in the 40 vol% disc (100–200 µm). Even so, the ALP values of the cells grown in the modified discs were somewhat lower than the untreated ones, which could indicate a greater differentiation of the cells. Most of the reported studies were carried out with in average growth periods shorter (1–4 days) than in this manuscript (21 days) and, therefore, greater cell differentiation was expected. Studies at 14 days did not report differences in ALP activity in MC3T3 cell cultures, showing results similar to those obtained in this work [52,53].

The morphological study of the MC3T3 osteoblast cells cultured on the different discs allowed observing that the growth in all of them was adequate and optimal, observing good cell adherence and a good biological response (Fig. 10). SEM images provided information on spatial distribution, cell morphology, cell-cell interaction, and cell-material surface interaction.

In all cultures it was observed cells with cuboidal shape and long elongated cytoplasmic processes (filopodia, marked with yellow arrow

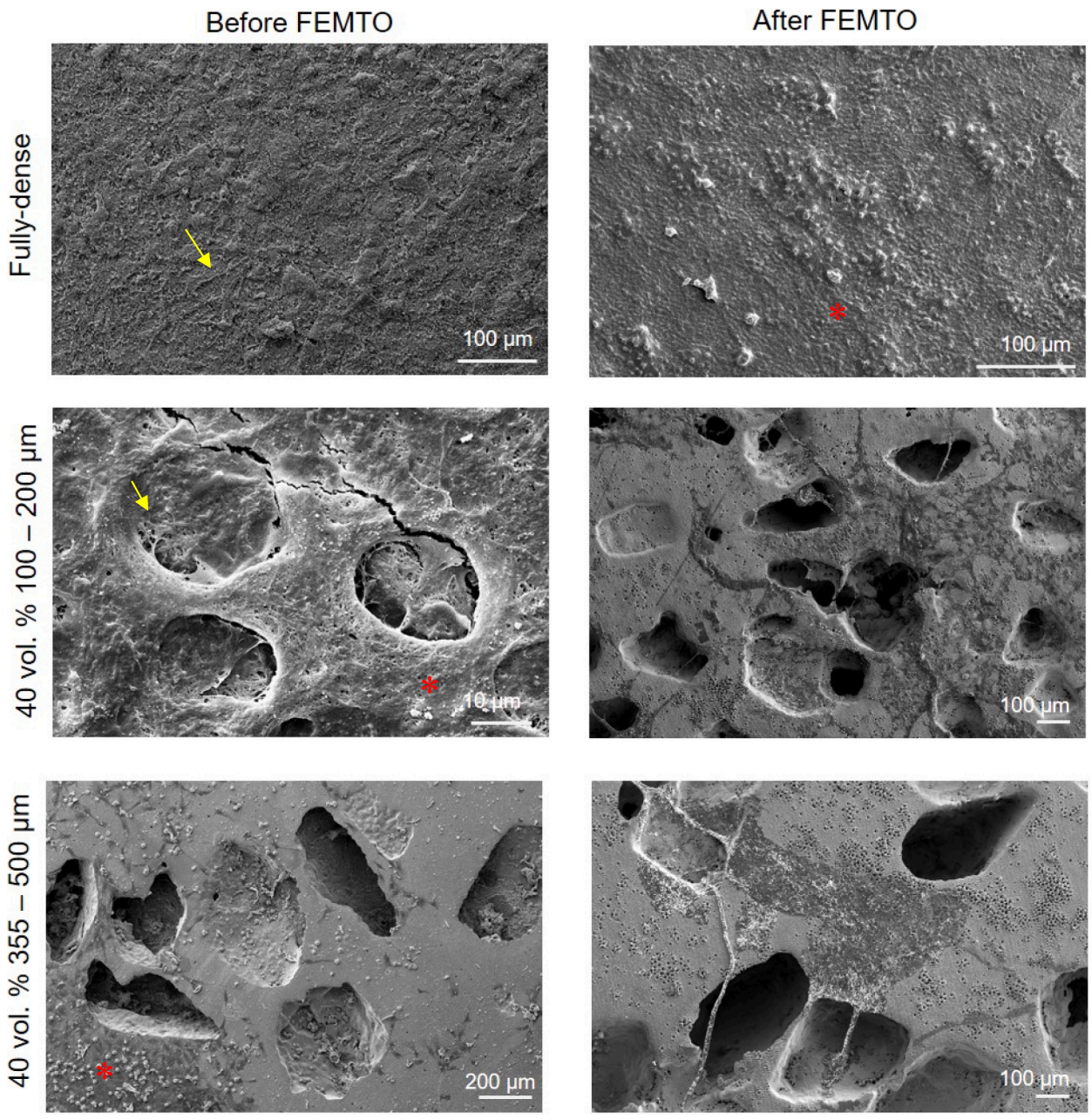

Fig. 10. SEM images of the cell adherence of the fully-dense and porous c.p. Ti before and after the femtosecond laser treatment. Cell–cell interaction, filopodia (yellow arrow) and hydroxyapatite (red asterisks) are indicated in the images.

in Fig. 10). The number of filopodia varied according to cell confluence, but it was high in all cases as the cells were widely spread on the surface [54]. In fully-dense discs, with and without femtosecond laser treatment, cell growth was clearly observed widely spread as a monolayer over the entire surface as well as deposits of Ca and hydroxyapatite (red asterisk are indicated in the images 10). The osteoblastic phenotype was typical of a highly differentiated cell and in the functional stage of mineralization [1,53,54]. As other authors have reported [52,55], cell growth inside the pores and the formation of connections among them were observed.

4. Conclusions

The microstructural, tribo-mechanical and cellular studies performed on superficially modified fully-dense and porous c.p. Ti discs with a femtosecond laser radiation allowed indicating the following general conclusions:

- The modification with the femtosecond laser generated an increase in the surface roughness of the Ti discs (nanometric ripples and micrometric-sized pillars areas) and increased the irregularity of the macro-pore contours obtained with the spacer-holder technique.
- The micro-hardness and stiffness increased around the pillars and decreased with the increase in the size of the macro-pores. Scratch resistance and elastic recovery were directly proportional to surface hardness and the role of micro- and macro-porosity.
- Surface modification with femtosecond laser treatment improved cell viability, mainly in fully-dense disc. A lower ALP activity in the treated samples could indicate a greater differentiation of the cells. The cell culture was similar in all cases, observing that modified discs presented a more differentiated morphology and an optimal cell adherence and acceptable biological response. It would be

convenient to perform further studies with other markers of medium and late expression, such as osteocalcin, bone sialoprotein to verify the effect of greater cell differentiation and greater mineralization in discs with modified surface.

In summary, in view of the obtained results, the use of femtosecond laser modified discs with a pore size of 100–200 μm is recommended, since they present better biomechanical behavior (stiffness, microhardness, mechanical and scratch resistance) and biofunctional behavior (bone ingrowth and cellular behavior), making them good candidates for bone tumor replacement.

CRediT authorship contribution statement

Paloma Trueba: Conceptualization, Methodology, Investigation, Data curation, Writing – original draft. **Mercè Giner:** Conceptualization, Methodology, Investigation, Writing – original draft. **Ángel Rodríguez:** Conceptualization, Methodology, Investigation, Data curation, Writing – original draft. **Ana M. Beltrán:** Conceptualization, Methodology, Investigation, Writing – original draft. **José M. Amado:** Conceptualization, Methodology, Investigation, Writing – review & editing. **María J. Montoya-García:** Conceptualization, Methodology, Investigation, Data curation, Writing – review & editing. **Luisa M. Rodríguez-Albelo:** Formal analysis, Methodology, Data curation, Investigation. **Yadir Torres:** Conceptualization, Methodology, Writing – review & editing, Supervision, Project administration, Funding acquisition.

Declaration of competing interest

The authors declare that they have no known competing financial interests or personal relationships that could have appeared to influence the work reported in this paper.

Acknowledgment

This work was supported by the Ministry of Science and Innovation of Spain under the grant PID2019-109371GB-I00, by the Junta de Andalucía–FEDER (Spain) through the Project Ref. US-1259771. Authors also thank to the technician J. Pinto for his support for the tribomechanical tests.

References

[1] Q. Chen, G.A. Thouas, Metallic implant biomaterials, Mater. Sci. Eng. R. Rep. 87 (2015) 1–57, https://doi.org/10.1016/j.mser.2014.10.001.
[2] D.M. Brunette, P. Tengvall, M. Textor, P. Thomsen, Titanium in Medicine: Material Science, Surface Science, Engineering, Biological Responses and Medical Applications, Springer Science & Business Media, 2012, https://doi.org/10.1007/978-3-642-56486-4.
[3] Y. Li, C. Yang, H. Zhao, S. Qu, X. Li, Y. Li, New developments of Ti-based alloys for biomedical applications, Materials 7 (2014) 1709–1800, https://doi.org/10.3390/ma7031709.
[4] R. Van Noort, Titanium: the implant material of today, J. Mater. Sci. 22 (1987) 3801–3811, https://doi.org/10.1007/BF01133326.
[5] M. Niinomi, Mechanical biocompatibilities of titanium alloys for biomedical applications, J. Mech. Behav. Biomed. Mater. 1 (2008) 30–42, https://doi.org/10.1016/j.jmbbm.2007.07.001.
[6] A.F. Mavrogenis, R. Dimitriou, J. Parvizi, G.C. Babis, Biology of implant osseointegration, J. Musculoskelet. Neuronal Interact. 9 (2009) 61–71.
[7] K. Pa\lka, R. Pokrowiecki, Porous titanium implants: a review, Adv. Eng. Mater. 20 (2018), 1700648, https://doi.org/10.1002/adem.201700648.
[8] Y. Torres, J. Pavón, I. Nieto, J. Rodríguez, Conventional powder metallurgy process and characterization of porous titanium for biomedical applications, Metall. Mater. Trans. B Process Metall. Mater. Process. Sci. 42 (2011) 891–900, https://doi.org/10.1007/s11663-011-9521-6.
[9] I.-H. Oh, N. Nomura, N. Masahashi, S. Hanada, Mechanical properties of porous titanium compacts prepared by powder sintering, Scr. Mater. 49 (2003) 1197–1202, https://doi.org/10.1016/j.scriptamat.2003.08.018.
[10] F. Matassi, A. Botti, L. Sirleo, C. Carulli, M. Innocenti, Porous metal for orthopedics implants, Clin. Cases Miner. Bone Metab. 10 (2013) 111–115.
[11] H. Schliephake, F.W. Neukam, D. Klosa, Influence of pore dimensions on bone ingrowth into porous hydroxylapatite blocks used as bone graft substitutes: a histometric study, Int. J. Oral Maxillofac. Surg. 20 (1991) 53–58, https://doi.org/10.1016/S0901-5027(05)80698-8.
[12] H.U. Camron, R.M. Pilliar, I. Macnab, The rate of bone ingrowth into porous metal, J. Biomed. Mater. Res. 10 (1976) 295–302, https://doi.org/10.1002/jbm.820100210.
[13] S.F. Hulbert, S.J. Morrison, J.J. Klawitter, Tissue reaction to three ceramics of porous and non-porous structures, J. Biomed. Mater. Res. 6 (1972) 347–374, https://doi.org/10.1002/jbm.820060505.
[14] X.-Y. Zhang, G. Fang, S. Leeflang, A.A. Zadpoor, J. Zhou, Topological design, permeability and mechanical behavior of additively manufactured functionally graded porous metallic biomaterials, Acta Biomater. 84 (2019) 437–452, https://doi.org/10.1016/j.actbio.2018.12.013.
[15] Y.Z. Yang, J.M. Tian, J.T. Tian, Z.Q. Chen, X.J. Deng, D.H. Zhang, Preparation of graded porous titanium coatings on titanium implant materials by plasma spraying, J. Biomed. Mater. Res. Off. J. Soc. Biomater. Jpn. Soc. Biomater. Aust. Soc. Biomater. Korean Soc. Biomater. 52 (2000) 333–337, https://doi.org/10.1002/1097-4636(200011)52:2<333::AID-JBM12>3.0.CO;2-T.
[16] A. Wennerberg, T. Albrektsson, Effects of titanium surface topography on bone integration: a systematic review, Clin. Oral Implants Res. 20 (2009) 172–184, https://doi.org/10.1111/j.1600-0501.2009.01775.x.
[17] Y. Wu, J.P. Zitelli, K.S. TenHuisen, X. Yu, M.R. Libera, Differential response of Staphylococci and osteoblasts to varying titanium surface roughness, Biomaterials. 32 (2011) 951–960, https://doi.org/10.1016/j.biomaterials.2010.10.001.
[18] X. Lu, Y. Leng, X. Zhang, J. Xu, L. Qin, C. Chan, Comparative study of osteoconduction on micromachined and alkali-treated titanium alloy surfaces in vitro and in vivo, Biomaterials. 26 (2005) 1793–1801, https://doi.org/10.1016/j.biomaterials.2004.06.009.
[19] Z. Schwartz, R. Olivares-Navarrete, M. Wieland, D.L. Cochran, B.D. Boyan, Mechanisms regulating increased production of osteoprotegerin by osteoblasts cultured on microstructured titanium surfaces, Biomaterials. 30 (2009) 3390–3396, https://doi.org/10.1016/j.biomaterials.2009.03.047.
[20] X. Zhu, J. Chen, L. Scheideler, R. Reichl, J. Geis-Gerstorfer, Effects of topography and composition of titanium surface oxides on osteoblast responses, Biomaterials. 25 (2004) 4087–4103, https://doi.org/10.1016/j.biomaterials.2003.11.011.
[21] V.D. Rani, L. Vinoth-Kumar, V.C. Anitha, K. Manzoor, M. Deepthy, V. N. Shantikumar, Osteointegration of titanium implant is sensitive to specific nanostructure morphology, Acta Biomater. 8 (2012) 1976–1989, https://doi.org/10.1016/j.actbio.2012.01.021.
[22] L. Salou, A. Hoornaert, G. Louarn, P. Layrolle, Enhanced osseointegration of titanium implants with nanostructured surfaces: an experimental study in rabbits, Acta Biomater. 11 (2015) 494–502, https://doi.org/10.1016/j.actbio.2014.10.017.
[23] T.J. Webster, C. Ergun, R.H. Doremus, R.W. Siegel, R. Bizios, Specific proteins mediate enhanced osteoblast adhesion on nanophase ceramics, J. Biomed. Mater. Res. Off. J. Soc. Biomater. Jpn. Soc. Biomater. Aust. Soc. Biomater. Korean Soc. Biomater. 51 (2000) 475–483, https://doi.org/10.1002/1097-4636(20000905)51:3<475::AID-JBM23>3.0.CO;2-9.
[24] K.C. Popat, L. Leoni, C.A. Grimes, T.A. Desai, Influence of engineered titania nanotubular surfaces on bone cells, Biomaterials. 28 (2007) 3188–3197, https://doi.org/10.1016/j.biomaterials.2007.03.020.
[25] S. Lavenus, M. Berreur, V. Trichet, P. Pilet, G. Louarn, P. Layrolle, Adhesion and osteogenic differentiation of human mesenchymal stem cells on titanium nanopores, Eur. Cell. Mater. 22 (2011) 84–96, https://doi.org/10.22203/ECM.V022A07.
[26] M.J. Dalby, N. Gadegaard, R. Tare, A. Andar, M.O. Riehle, P. Herzyk, C. D. Wilkinson, R.O. Oreffo, The control of human mesenchymal cell differentiation using nanoscale symmetry and disorder, Nat. Mater. 6 (2007) 997–1003, https://doi.org/10.1038/nmat2013.
[27] G. Colon, B.C. Ward, T.J. Webster, Increased osteoblast and decreased Staphylococcus epidermidis functions on nanophase ZnO and TiO2, J. Biomed. Mater. Res. Off. J. Soc. Biomater. Jpn. Soc. Biomater. Aust. Soc. Biomater. Korean Soc. Biomater. 78 (2006) 595–604, https://doi.org/10.1002/jbm.a.30789.
[28] S.D. Puckett, E. Taylor, T. Raimondo, T.J. Webster, The relationship between the nanostructure of titanium surfaces and bacterial attachment, Biomaterials. 31 (2010) 706–713, https://doi.org/10.1016/j.biomaterials.2009.09.081.
[29] R.G. Flemming, C.J. Murphy, G.A. Abrams, S.L. Goodman, P.F. Nealey, Effects of synthetic micro-and nano-structured surfaces on cell behavior, Biomaterials. 20 (1999) 573–588, https://doi.org/10.1016/S0142-9612(98)00209-9.
[30] A.S.G. Curtis, B. Casey, J.O. Gallagher, D. Pasqui, M.A. Wood, C.D.W. Wilkinson, Substratum nanotopography and the adhesion of biological cells. Are symmetry or regularity of nanotopography important? Biophys. Chem. 94 (2001) 275–283, https://doi.org/10.1016/S0301-4622(01)00247-2.
[31] M. Kaur, K. Singh, Review on titanium and titanium based alloys as biomaterials for orthopaedic applications, Mater. Sci. Eng. C 102 (2019) 844–862, https://doi.org/10.1016/j.msec.2019.04.064.
[32] M.J. Biggs, R.G. Richards, N. Gadegaard, C.D.W. Wilkinson, M.J. Dalby, Regulation of implant surface cell adhesion: characterization and quantification of S-phase primary osteoblast adhesions on biomimetic nanoscale substrates, J. Orthop. Res. 25 (2007) 273–282, https://doi.org/10.1002/jor.20319.
[33] A. Kurella, N.B. Dahotre, Surface modification for bioimplants: the role of laser surface engineering, J. Biomater. Appl. 20 (2005) 5–50, https://doi.org/10.1177/0885328205052974.
[34] R. Kumari, T. Scharnweber, W. Pfleging, H. Besser, J.D. Majumdar, Laser surface textured titanium alloy (Ti–6Al–4V)–part II–studies on bio-compatibility, Appl, Surf. Sci. 357 (2015) 750–758, https://doi.org/10.1016/j.apsusc.2015.08.255.

[35] A. Gaggl, G. Schultes, W.D. Müller, H. Kärcher, Scanning electron microscopical analysis of laser-treated titanium implant surfaces—a comparative study, Biomaterials. 21 (2000) 1067–1073, https://doi.org/10.1016/S0142-9612(00)00002-8.
[36] K.C. Phillips, H.H. Gandhi, E. Mazur, S.K. Sundaram, Ultrafast laser processing of materials: a review, Adv. Opt. Photon. 7 (2015) 684–712, https://doi.org/10.1364/AOP.7.000684.
[37] R. Le Harzic, N. Huot, E. Audouard, C. Jonin, P. Laporte, S. Valette, A. Fraczkiewicz, R. Fortunier, Comparison of heat-affected zones due to nanosecond and femtosecond laser pulses using transmission electronic microscopy, Appl. Phys. Lett. 80 (2002) 3886–3888, https://doi.org/10.1063/1.1481195.
[38] D. Breitling, A. Ruf, F. Dausinger, Fundamental aspects in machining of metals with short and ultrashort laser pulses, in: Photon Process. Microelectron. Photonics III, International Society for Optics and Photonics, 2004, pp. 49–63, https://doi.org/10.1117/12.541434.
[39] X. Liu, D. Du, G. Mourou, Laser ablation and micromachining with ultrashort laser pulses, IEEE J. Quantum Electron. 33 (1997) 1706–1716, https://doi.org/10.1109/3.631270.
[40] K.M.T. Ahmmed, C. Grambow, A.-M. Kietzig, Fabrication of micro/nano structures on metals by femtosecond laser micromachining, Micromachines. 5 (2014) 1219–1253, https://doi.org/10.3390/mi5041219.
[41] Á. Rodríguez, P. Trueba, J.M. Amado, M.J. Tobar, M. Giner, V. Amigó, Y. Torres, Surface modification of porous titanium discs using femtosecond laser structuring, Metals 10 (2020) 748, https://doi.org/10.3390/met10060748.
[42] Y. Torres, J.J. Pavón, J.A. Rodríguez, Processing and characterization of porous titanium for implants by using NaCl as space holder, J. Mater. Process. Technol. 212 (2012) 1061–1069, https://doi.org/10.1016/j.jmatprotec.2011.12.015.
[43] Y. Torres, P. Trueba, J.J. Pavón, E. Chicardi, P. Kamm, F. García-Moreno, J. A. Rodríguez-Ortiz, Design, processing and characterization of titanium with radial graded porosity for bone implants, Mater. Des. 110 (2016) 179–187, https://doi.org/10.1016/j.matdes.2016.07.135.
[44] W.C. Oliver, G.M. Pharr, Measurement of hardness and elastic modulus by instrumented indentation: advances in understanding and refinements to methodology, J. Mater. Res. 19 (2004) 3–20, https://doi.org/10.1557/jmr.2004.19.1.3.
[45] ASTM C1624-05, Standard Test Method for Adhesion Strength and Mechanical Failure Modes of Ceramic Coatings by Quantitative Single Point Scratch Testing 2015, ASTM International, West Conshohocken, PA, 2015, https://doi.org/10.1520/C1624-05R15.
[46] Q. Huang, T.A. Elkhooly, X. Liu, R. Zhang, X. Yang, Z. Shen, Q. Feng, Effects of hierarchical micro/nano-topographies on the morphology, proliferation and differentiation of osteoblast-like cells, Colloids Surf. B: Biointerfaces 145 (2016) 37–45, https://doi.org/10.1016/j.colsurfb.2016.04.031.
[47] L. Zhao, S. Mei, P.K. Chu, Y. Zhang, Z. Wu, The influence of hierarchical hybrid micro/nano-textured titanium surface with titania nanotubes on osteoblast functions, Biomaterials. 31 (2010) 5072–5082, https://doi.org/10.1016/j.biomaterials.2010.03.014.
[48] J. Gaviria, A. Alcudia, B. Begines, A.M. Beltrán, J. Villarraga, R. Moriche, J. A. Rodríguez-Ortiz, Y. Torres, Synthesis and deposition of silver nanoparticles on porous titanium substrates for biomedical applications, Surf. Coat. Technol. 406 (2021), 126667, https://doi.org/10.1016/j.surfcoat.2020.126667.
[49] P. Goegan, G. Johnson, R. Vincent, Effects of serum protein and colloid on the alamarBlue assay in cell cultures, Toxicol. in Vitro 9 (1995) 257–266, https://doi.org/10.1016/0887-2333(95)00004-R.
[50] S. Shaikh, D. Singh, M. Subramanian, S. Kedia, A.K. Singh, K. Singh, N. Gupta, S. Sinha, Femtosecond laser induced surface modification for prevention of bacterial adhesion on 45S5 bioactive glass, J. Non-Cryst. Solids 482 (2018) 63–72.
[51] C. Liang, H. Wang, J. Yang, Y. Cai, X. Hu, Y. Yang, B. Li, H. Li, H. Li, C. Li, Femtosecond laser-induced micropattern and Ca/P deposition on Ti implant surface and its acceleration on early osseointegration, ACS Appl. Mater. Interfaces 5 (2013) 8179–8186, https://doi.org/10.1021/am402290e.
[52] A. Civantos, M. Giner, P. Trueba, S. Lascano, M.-J. Montoya-García, C. Arévalo, M.Á. Vázquez, J.P. Allain, Y. Torres, In vitro bone cell behavior on porous titanium samples: influence of porosity by loose sintering and space holder techniques, Metals. 10 (2020) 696, https://doi.org/10.3390/met10050696.
[53] Y. Liu, Z. Rui, W. Cheng, L. Song, Y. Xu, R. Li, X. Zhang, Characterization and evaluation of a femtosecond laser-induced osseointegration and an anti-inflammatory structure generated on a titanium alloy, Regen. Biomater. 8 (2021), https://doi.org/10.1093/rb/rbab006 rbab006.
[54] G. Schnell, S. Staehlke, U. Duenow, J.B. Nebe, H. Seitz, Femtosecond laser nano/micro textured Ti6Al4V surfaces—effect on wetting and MG-63 cell adhesion, Materials 12 (2019) 2210, https://doi.org/10.3390/ma12132210.
[55] A.C. Alves, R. Thibeaux, F. Toptan, A.M.P. Pinto, P. Ponthiaux, B. David, Influence of macroporosity on NIH/3T3 adhesion, proliferation, and osteogenic differentiation of MC3T3-E1 over bio-functionalized highly porous titanium implant material, J Biomed Mater Res B Appl Biomater 107 (2019) 73–85, https://doi.org/10.1002/jbm.b.34096.